Dalton Transactions

ROYAL SOCIETY OF CHEMISTRY

PAPER

View Article Online
View Journal | View Issue

Cite this: *Dalton Trans.*, 2025, **54**, 18117

Indium alkoxide complexes supported by constrained Schiff-base ligands for the ring-opening (co)polymerization of cyclic esters

Thitirat Piyawongsiri, Phongnarin Chumsaeng and Khamphee Phomphrai *

Received 1st October 2025,
Accepted 10th November 2025

DOI: 10.1039/d5dt02356d

rsc.li/dalton

Indium *tert*-butoxide complexes supported by constrained Schiff-base ligands with different diamine backbones were successfully synthesized (**2a–c**) and developed for the ring-opening polymerization (ROP) of lactide (LA), glycolide (GA) and ε-caprolactone (CL). Single-crystal X-ray studies reveal that all complexes are monomeric containing a five-coordinate indium metal center. All complexes were highly active for ROP of cyclic esters. The indium *tert*-butoxide complex having a *trans*-cyclohexyl backbone (**2c**) showed very high activities finishing 98% conversion of 200 equiv. of L-lactide (L-LA) in 3 min at room temperature (TOF = 3920 h^{-1}). Polymerization of *rac*-LA gave stereoblock isotactic-enriched PLA with P_m values of up to 0.85. The kinetic studies of the ROP of cyclic esters revealed a pseudo first-order dependence with respect to monomer concentrations and the rate order of *rac*-LA ≈ D-LA > L-LA ≫ CL. From the studies of monomer reactivity ratios using complex **2c**, the copolymerization of LA with GA gave block copolymers while the copolymerization of LA with CL gave gradient copolymers.

Introduction

In recent years, plastic pollution has become one of the most pressing environmental issues due to the rapidly increasing production of disposable plastic products. Therefore, biodegradable polymers have received much attention due to their safe biodegradation in natural environments.[1] Some of the most important biodegradable polymers are aliphatic polyesters. Many of them show outstanding biodegradability and biocompatibility. Ring-opening polymerization (ROP) of cyclic esters is one of the most effective and common synthetic pathways to produce aliphatic polyesters. Aliphatic polyesters such as polyglycolide (PGA), poly(lactide) (PLA), and poly(caprolactone) (PCL) have attracted considerable attention as a promising green alternative to petrochemically derived polymers[2–8] with excellent applications in packaging[9–12] and biomedical applications.[13–18]

Several metal complexes[19–28] such as Mg, Zn, Sn, Cr, and Al have been investigated and shown to be effective catalysts for the ROP of cyclic esters.[29–31] Among them, indium, a relatively soft Lewis acid with low toxicity and high oxophilicity,[32,33] is well known as a well-behaved catalyst which has demonstrated high activity and stereoselectivity for several monomers.[34–40] For example, a simple indium(III) chloride catalyst system used for the ROP of *rac*-lactide (*rac*-LA) shows stereoselective and controlled polymerizations towards heterotactic PLA.[41,42] However, polymerization rates were relatively moderate. Therefore, the development of indium complexes has garnered considerable attention to increase the activities in the ROP of cyclic esters (Fig. 1). In 2015, indium catalysts supported by ferrocenylsalen (salfen)In(O^{t}Bu) (**A**) were reported for ROP of cyclic esters. (Salfen)In(O^{t}Bu) could catalyze the polymerization of 100 equiv. of L-lactide (L-LA), achieving 95% conversion in 4.5 h, and 100 equiv. of ε-caprolactone (CL) achieving 99% conversion in just 2 min. These results highlighted (salfen)In(O^{t}Bu) as the fastest indium-based catalyst for lactone polymerization.[37] Later in 2022, studies of the indium salan (**B**) complex developed by Rieger revealed that catalysts with a flexible ligand framework exhibit higher activity than those with a more constrained framework for ROP of cyclic esters.[40] Williams reported the phosphasalen indium complex (**C**) showing high rates and isoselectivity for *rac*-LA ROP (P_m > 0.75, at 25 °C, TOF of 160 h^{-1}).[35,43] The chiral indium salen complex (**D**) reported by Mehrkhodavandi also showed high rates and good isoselectivity (P_m = 0.77).[44]

Recently, our group reported indium chloride complexes supported by constrained Schiff-base ligands (inden) for the formation of cyclic carbonates from epoxides and CO_2.[45] The constrained 5-membered rings on the inden structure enlarge the coordination site on the metal center resulting in good catalytic activity with a turnover number (TON) of up to 1018.

Department of Materials Science and Engineering, School of Molecular Science and Engineering, Vidyasirimedhi Institute of Science and Technology (VISTEC), Wangchan, Rayong 21210, Thailand. E-mail: khamphee.p@vistec.ac.th

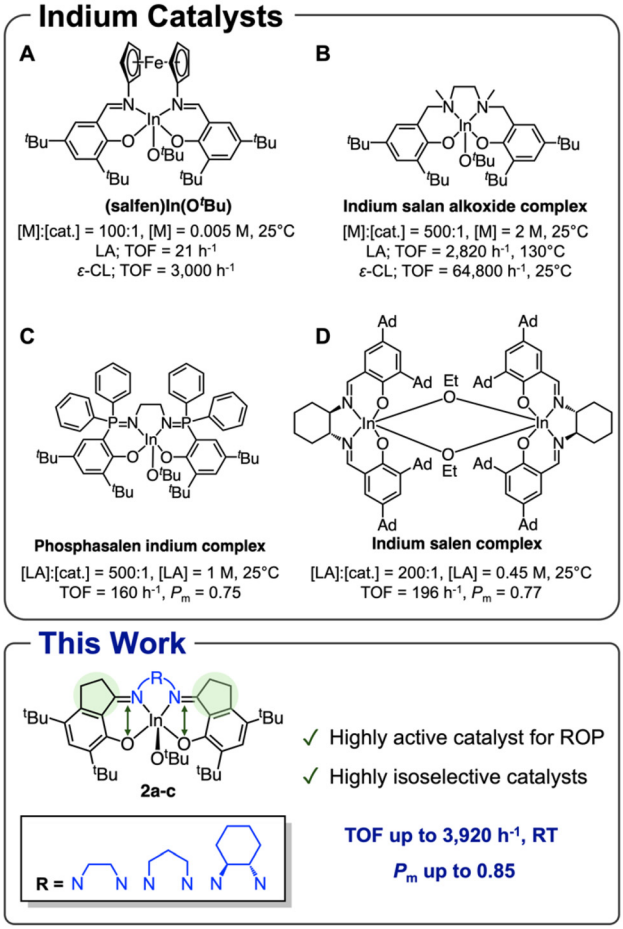

Fig. 1 Structures of catalysts A–D for ROP of cyclic esters.[35,37,40,43,44]

A similar effect of constrained inden was observed in the chromium and aluminum inden complexes resulting in very high activities for the coupling reaction of epoxies/CO_2 and ring-opening co(ter)polymerization of epoxides/cyclic anhydrides and lactide.[46–48]

With the success of the constrained inden metal complexes, we extended the constrained inden ligand framework to indium metal for ROP of cyclic esters for the first time. Herein, we have developed a series of indium alkoxide complexes supported by the inden ligand for the ROP of cyclic esters including LA, GA, and CL to produce well-defined aliphatic polyesters along with the studies of polymer tacticity, kinetic studies, and their copolymers.

Experimental

Materials

All operations involving air- or moisture-sensitive reactions were carried out in a glovebox or using a standard Schlenk technique under a nitrogen atmosphere. Tetrahydrofuran (THF), *n*-hexane, benzene, toluene, and dichloromethane were dried using a solvent purification system (MB SPS-800, MBRAUN). The lactide monomer was recrystallized from toluene and purified by sublimation under vacuum 3 times before use and stored in a refrigerator in a glovebox. The ε-caprolactone (CL) monomer was dried over calcium hydride, distilled under vacuum, and stored in a refrigerator in a glovebox. Other solvents and chemicals were obtained from commercial suppliers and used as received. Ligands **1a**, **1b** and **1c** were synthesized according to a literature procedure.[45]

Measurements

^{1}H and ^{13}C NMR spectra were recorded on a Bruker AVANCE III HD-600 MHz spectrometer and referenced to the protio impurity of commercial benzene-d_6 (C_6D_6, δ 7.16 ppm), chloroform-d ($CDCl_3$, δ 7.26 ppm), and dimethyl sulfoxide-d_6 (DMSO-d_6, δ 2.50 ppm) as internal standards. For air-sensitive NMR samples, solvents were dried over 4 Å molecular sieves and used in Teflon-valve-sealed J. Young-type NMR tubes. Matrix-assisted laser desorption and ionization time-of-flight (MALDI-TOF) mass spectra were obtained on a Bruker Daltonics Autoflex Speed TM mass spectrometer equipped with a laser frequency of 2000 Hz. Solutions of *trans*-2-[3-(4-*tert*-butylphenyl)-2-methyl-2-propylidene]-malononitrile (DCTB) (80 μL of a 40 mg L^{-1} DCM solution) used as the matrix, sodium iodide (20 μL of a 5 mg L^{-1} THF solution) as the cationization agent and a polymer (20 μL of a 1 mg L^{-1} THF solution) were mixed together and spotted onto the target plate, followed by solvent evaporation to prepare a thin polymer film. The samples were measured in linear positive mode with Protein Calibration Standard I. The M_n and dispersity ($Đ$) of polymers were analyzed using gel permeation chromatography (GPC) using THF as the eluent with a flow rate of 1.0 mL min^{-1} at 35 °C. The measurement was performed on a Malvern GPCmax instrument equipped with a refractive index detector and three 300 × 8.0 mm ID columns packed with a porous styrene divinylbenzene copolymer. The calibration curve was constructed with polystyrene standards ranging from 1200 to 4 200 000 amu. Elemental analyses were performed on an LECO TruSpec microelemental analyzer. Differential scanning calorimetry (DSC) measurements were performed on a PerkinElmer DSC-8500. Polymer samples were first heated to 250 °C at 10 °C min^{-1}, equilibrated at this temperature for 10 min, then cooled to −80 °C at 10 °C min^{-1}, held for 10 min, and reheated to 250 °C at 10 °C min^{-1} under a nitrogen atmosphere.

X-ray crystallography

The X-ray crystallographic data were collected on a Bruker D8 Venture using a Photon II detector and an IμS 3.0 microfocus source with Mo Kα radiation (λ = 0.71073 Å). Data collection was carried out using the Bruker APEX3 software suite. Data integration was performed with the SAINT software, and intensity data were corrected based on the intensities and symmetry-related reflections measured at different angular settings (SADABS). The space group was determined with the XPREP software. The crystal structures were solved by direct methods using intrinsic phasing (SHELXT program)[49] and

refined by full-matrix least squares against F^2 using the program SHELXL based on the ShelXle engine or Olex2 software package.[50] All non-H atoms were refined anisotropically, while the H atoms were placed in calculated positions and not refined. The crystallographic images were processed using the Ortep3 program.

Synthetic procedures for indium complexes

Complex 2a. The synthesis of complex **2a** follows a slightly modified literature procedure.[43] Ligand **1a** (500 mg, 0.920 mmol, 1.0 equiv.) was dissolved in THF, and NaH (44 mg, 1.84 mmol, 2.0 equiv.) was added to the flask. Formation of hydrogen gas was observed for about 2 h. After complete gas evolution, $InCl_3$ (203 mg, 0.920 mmol, 1.0 equiv.) was added. The reaction was stirred at room temperature overnight. Afterwards, the resulting solution was evaporated under reduced pressure. Dried benzene was added to the solid residue and stirred for 20 min. The resulting solution was filtered, and the solvent was removed under reduced pressure. The solid residue was confirmed to be ligated indium chloride by ^{1}H NMR spectroscopy at this stage.[45] A portion of NaO^{t}Bu (89 mg, 0.92 mmol, 1.0 equiv.) was then added as a solid. The reaction mixture was dissolved in benzene and then allowed to stir at room temperature overnight. The resulting solution was filtered to remove NaCl salt and then evaporated under reduced pressure. The product was washed with hexane and dried under reduced pressure to give a yellow powder (340 mg, 50% yield). ^{1}H NMR (600 MHz, C_6D_6, 30 °C): δ 7.75 (s, 2H, Ar–*H*), 3.32–3.25 (m, 2H, NCH_2), 2.80 (ddd, J = 16.4, 7.7, 3.8 Hz, 2H, Ar–CH_2), 2.71 (ddd, J = 16.4, 7.5, 5.0 Hz, 2H, Ar–CH_2), 2.62–2.53 (m, 2H, NCH_2), 1.89 (s, 18H, C(CH_3)$_3$), 1.85 (td, J = 7.1, 4.4 Hz, 4H, Ar–CH_2, Ar–CH_2), 1.57 (s, 9H, OC(CH_3)$_3$), 1.41 (s, 18H, C(CH_3)$_3$). ^{13}C NMR (150 MHz, C_6D_6, 30 °C): δ 185.60 (*C*═N), 166.91, 147.11, 139.66, 131.38, 131.06, 123.08 (*C*Ar), 69.69 (O*C*(CH$_3$)$_3$), 47.61 (N*C*H$_2$), 35.75 (*C*(CH$_3$)$_3$, 35.22 (*C*(CH$_3$)$_3$, OC(*C*H$_3$)$_3$), 31.17 ((*C*H$_3$)$_3$), 30.42 (Ar–*C*H$_2$), 30.25 ((*C*H$_3$)$_3$), 28.28 (Ar–*C*H$_2$). MALDI-ToF-MS: m/z [M − O^{t}Bu]$^+$: calculated 657.2911; found 657.6507. Anal. calcd for $C_{40}H_{59}InN_2O_3$: C, 65.75; H, 8.14; N, 3.83. Found: C, 65.70; H, 8.18; N, 3.96.

Complex 2b. The synthesis of complex **2b** follows the method for **2a** starting from ligand **1b** (514 mg, 0.92 mmol). The product was isolated as an orange powder after washing with hexane (330 mg, 48% yield). ^{1}H NMR (600 MHz, C_6D_6, 30 °C): δ 7.72 (s, 2H, Ar–*H*), 3.16 (td, J = 13.3, 3.5 Hz, 2H, NCH_2), 2.74 (t, J = 13.3 Hz, 2H, NCH_2), 2.69–2.60 (m, 4H, Ar–CH_2), 1.87 (s, 18H, C(CH_3)$_3$), 1.81 (dddd, J = 16.8, 11.2, 5.2, 2.6 Hz, 4H, Ar–CH_2), 1.70 (s, 9H, OC(CH_3)$_3$), 1.49–1.41 (m, 2H, N–CH$_2$–CH_2), 1.38 (s, 18H, C(CH_3)$_3$). ^{13}C NMR (150 MHz, C_6D_6, 30 °C): δ 187.60 (*C*═N), 167.43, 147.05, 139.10, 131.06, 130.84, 122.40 (*C*Ar), 70.06 (O*C*(CH$_3$)$_3$), 53.49 (N*C*H$_2$), 35.76 (*C*(CH$_3$)$_3$), 35.23 (OC(*C*H$_3$)$_3$), 35.14 (*C*(CH$_3$)$_3$), 31.24 (Ar–*C*H$_2$), 31.10 ((*C*H$_3$)$_3$), 30.53 ((*C*H$_3$)$_3$), 27.96 (*C*H$_2$), 27.92 (Ar–*C*H$_2$). MALDI-ToF-MS: m/z [M − O^{t}Bu]$^+$: calculated 671.3068; found 671.7153. Anal. calcd for $C_{41}H_{61}InN_2O_3$: C, 66.12; H, 8.26; N, 3.76. Found: C, 66.41; H, 8.68; N, 3.41.

Complex 2c. The synthesis of complex **2c** follows the method for **2a** starting from ligand **1c** (550 mg, 0.92 mmol). The product was isolated as a yellow powder after washing with hexane (325 mg, 45% yield). ^{1}H NMR (600 MHz, C_6D_6, 30 °C): δ 7.76 (s, 1H, Ar–*H*), 7.65 (s, 1H, Ar–*H*), 4.44 (t, J = 9.6 Hz, 1H, C═N–C*H*), 2.78 (ddd, J = 12.3, 7.1, 5.2 Hz, 2H, Ar–CH_2), 2.74–2.54 (m, 3H, C═N–C*H*–CH_2), 2.14 (t, J = 6.3 Hz, 2H, Ar–CH_2), 2.08 (ddd, J = 18.2, 8.5, 3.3 Hz, 2H, CH_2), 1.92 (s, 9H, C(CH_3)$_3$), 1.83 (s, 9H, OC(CH_3)$_3$), 1.76 (ddd, J = 18.5, 8.4, 3.7 Hz, 2H, CH_2), 1.71 (s, 9H, C(CH_3)$_3$), 1.53–1.47 (m, 2H, Ar–CH_2), 1.40 (d, J = 4.4 Hz, 18H, C(CH_3)$_3$), 1.14 (dd, J = 14.3, 5.4 Hz, 2H, CH_2), 0.94 (ddp, J = 26.6, 14.8, 7.7 Hz, 2H, Ar–CH_2). ^{13}C NMR (150 MHz, C_6D_6, 30 °C): δ 187.70, 180.65 (*C*═N), 167.47, 166.51, 146.80, 145.74, 139.44, 139.33, 131.17, 131.03, 131.01, 130.46, 124.39, 123.19 (*C*Ar), 70.22 (O*C*(CH$_3$)$_3$), 66.96, 65.17 (C═N–*C*H), 35.77 (OC(*C*H$_3$)$_3$), 35.71 (*C*(CH$_3$)$_3$), 35.23, 35.20 ((*C*H$_3$)$_3$), 32.15, 31.93, 31.45 (*C*H$_2$), 31.11, 31.09 ((*C*H$_3$)$_3$, *C*H$_2$), 30.51, 30.13 ((*C*H$_3$)$_3$), 28.61, 28.26, 25.76, 24.67 (Ar–*C*H$_2$). MALDI-ToF-MS: m/z [M − O^{t}Bu]$^+$: calculated 711.3381; found 711.7070. Anal. calcd for $C_{44}H_{65}InN_2O_3$: C, 67.34; H, 8.35; N, 3.57. Found: C, 67.06; H, 8.15; N, 3.64.

General (co)polymerization procedure at room temperature

The amounts of monomer, catalyst, and dichloromethane (DCM) were adjusted according to the monomer/catalyst mole ratio in the desired concentration. In a glovebox, a solution of catalyst was added to the solution of monomer in a reaction flask. The reaction flask was sealed and stirred at room temperature. At a specific time, a few drops of 10% benzoic acid solution were added to quench the reaction. A small aliquot was taken and analyzed by ^{1}H NMR spectroscopy to determine the conversion. The remaining mixture was concentrated under reduced pressure, and the resulting polymer was redissolved in a minimal volume of DCM. Precipitation was then carried out by adding the resulting polymer solution into an excess of cold methanol. After decanting the supernatant, the polymer was dried under vacuum to a constant weight and subsequently analyzed by NMR spectroscopy, gel permeation chromatography (GPC) and/or MALDI-TOF mass spectrometry.

General polymerization procedure at low temperature

The initial *rac*-LA concentration of 0.10 M in DCM was used in a 100 : 1 *rac*-LA to catalyst ratio. In a glovebox, a pre-cooled solution of the catalyst was added to a pre-cooled solution of the monomer in a reaction flask at −30 °C. The reaction flask was sealed and kept at −30 °C. At a specific time, a few drops of benzoic acid solution (10% benzoic acid in DCM) were added to quench the reaction. A small amount of sample was taken and analyzed by ^{1}H NMR spectroscopy to determine the conversion. The remaining mixture was concentrated under vacuum, and the polymer was redissolved in a minimum amount of DCM and then precipitated with excess cold methanol. The supernatant was decanted off, and the polymer was dried under vacuum to constant weight followed by analysis with NMR spectroscopy and gel permeation chromatography (GPC).

Results and discussion

Catalyst synthesis and characterization

Previous indium catalysts supported by inden ligands having various substitution groups at the aromatic rings were reported for epoxide/CO_2 cycloaddition reaction.[45] The indium catalyst with a ligand containing *tert*-butyl groups showed good solubility in organic solvent and higher catalytic activity than others. Therefore, the *tert*-butyl groups were selected as the substituents in this work. The focus was then placed on the constraint at the backbone of the ligand framework to understand how this may affect the catalytic activities. A series of indium alkoxide complexes was synthesized in moderate yield having different diamine backbones (**2a–c**). The complexes were prepared from the inden ligands (**1a–c**; R = $-(CH_2)_2-$, $-(CH_2)_3-$, *trans*-cyclohexyl) by a deprotonation reaction using NaH, followed by the reaction with $InCl_3$. The resulting indium chloride complexes were then reacted with NaO^tBu to form the desired indium *tert*-butoxide complexes **2a–2c** (Scheme 1).

Single crystals of complexes **2a–2c** were obtained from a vapor diffusion method between benzene and hexane. The molecular structures of **2a–2c** were determined by single-crystal X-ray crystallography, as shown in Fig. 2–4, respectively. All complexes are monomeric 5-coordinated indium center containing a *tert*-butoxide ligand. In contrast to other indium alkoxide complexes which are dimeric due to the large size of the metal,[51,52] steric hindrance from the *tert*-butyl and *tert*-butoxide groups likely stabilizes the complexes to be monomeric. The geometry indices (τ_5) of indium *tert*-butoxide complexes are in the order **2a** (τ = 0.018) < **2c** (τ = 0.430) < **2b** (τ = 0.622).[53] Complex **2a** (R = $-(CH_2)_2-$) has a square-based pyramidal geometry (Fig. 2), while **2c** (R = *trans*-cyclohexyl) has an intermediate structure between a square-based pyramidal and trigonal bipyramidal geometry. On the other hand, complex **2b** (R = $-(CH_2)_3-$) containing a rather flexible diamine backbone has a distorted trigonal bipyramidal geometry. The presence of the five-membered ring of the inden ligand led to significantly longer average N–O distances (*e.g.* N1–O1, N2–O2) in complex **2c** (ave. 2.925 Å) compared to the non-constraint ((salen)In(OEt))$_2$ (ave. 2.870 Å).[52] It is noteworthy that the size of the attached ring could directly influence the distance between the two coordinating atoms. For example, the O–O distances in the related keto-phenol containing the 5-, 6-, and 7-membered rings are 2.899, 2.494, and 2.544 Å, respectively (see Fig. S1).[54–56] In this series, the 5-membered ring gives the longest O–O distance allowing a wider coordinating sphere around the metal. The distance between In–O (*i.e.* In1–O3) of 2.025 Å for **2a** and **2b** is slightly longer than 2.001 Å for **2c**. However, all values still fall within the reported range for other monomeric indium alkoxide complexes (1.987–2.025 Å).[35,40,43] This suggests that the In–O bonds are comparable to other reported indium alkoxide complexes. Moreover, the bite angles (*e.g.* N1–In–O1 and N2–In–O2 bond angles) in **2c** (ave. 85.74°) are wider compared to that of non-constrained ((salen)In(OEt))$_2$ which is less than 85° (ave. 82.85°).[52] Therefore, it is evident that the constraint of the 5-membered rings in inden ligands could provide more space at the metal center allowing better substrate coordination.

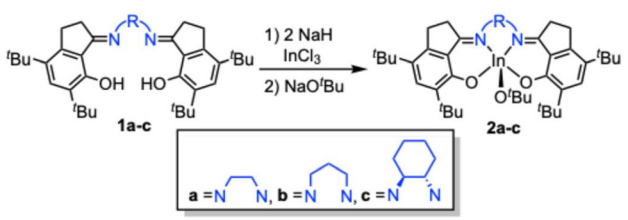

Scheme 1 Synthesis of indium complexes supported by inden ligands (**2a–2c**).

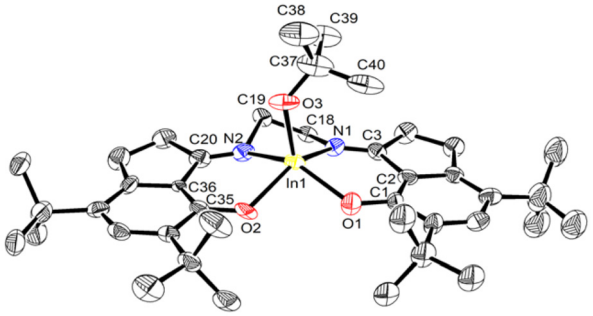

Fig. 2 Molecular structure (ORTEP) of **2a** with thermal ellipsoids drawn at the 50% probability level. Solvent and hydrogen atoms are omitted for clarity. Selected bond distances (Å) and angles (°): In1–O3 2.026(7), In1–O1 2.060(8), In1–O2 2.089(7), In1–N1 2.207(8), In1–N2 2.207(1), N2–O2 2.903(1), N1–O1 2.905(1), O3–In1–O1 115.7(4), O3–In1–O2 104.4(4), O3–In1–N1 111.5(4), O3–In1–N2 101.2(4), O1–In1–O2 91.0(3), N2–In1–O2 85.0(3), N1–In1–N2 75.2(3), O1–In1–N1 85.7(3), N2–In1–O1 142.6(4), N1–In1–O2 141.5(4).

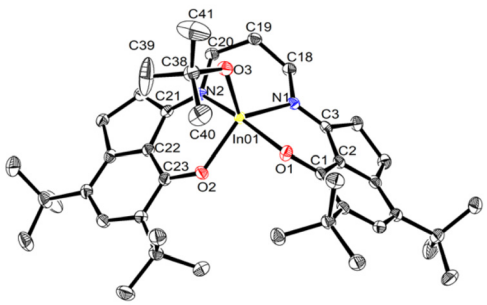

Fig. 3 Molecular structure (ORTEP) of **2b** with thermal ellipsoids drawn at the 50% probability level. Solvent and hydrogen atoms are omitted for clarity. Selected bond distances (Å) and angles (°): In1–O3 2.025(9), In1–O1 2.107(9), In1–O2 2.092(9), In1–N1 2.194(1), In1–N2 2.259(1), N2–O2 2.950(1), N1–O1 2.909(1), O3–In1–O1 100.2(4), O3–In1–O2 120.9(4), O3–In1–N1 113.5(4), O3–In1–N2 96.6(4), O1–In1–O2 89.3(4), N2–In1–O2 85.3(4), N1–In1–N2 84.7(4), O1–In1–N1 85.1(4), N2–In1–O1 162.7(4), N1–In1–O2 125.4(4).

Ring-opening polymerization of cyclic esters

All indium *tert*-butoxide complexes were investigated for the ROP of cyclic esters toward L-lactide (L-LA), glycolide (GA) and

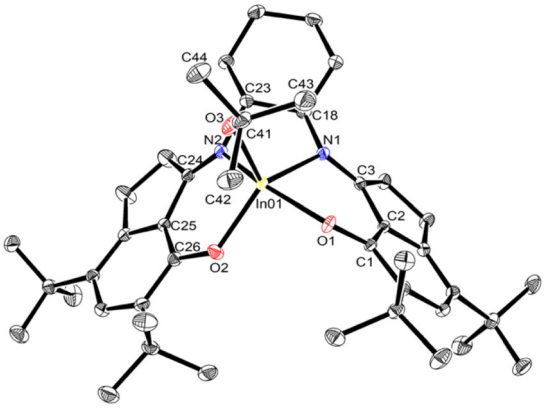

Fig. 4 Molecular structure (ORTEP) of **2c** with thermal ellipsoids drawn at the 50% probability level. Both racemic mixtures of **2c** are formed. Only (*R*,*R*)-**2c** is shown here. Solvent and hydrogen atoms are omitted for clarity. Selected bond distances (Å) and angles (°): In1–O3 2.001(2), In1–O1 2.083(2), In1–O2 2.057(2), In1–N1 2.219(2), In1–N2 2.232(2), N2–O2 2.952(1), N1–O1 2.898(1), O3–In1–O1 109.2(8), O3–In1–O2 116.7(9), O3–In1–N1 112.8(9), O3–In1–N2 93.3(8), O1–In1–O2 95.9(7), N2–In1–O2 86.8(8), N1–In1–N2 72.5(8), O1–In1–N1 84.6(7), N2–In1–O1 152.9(8), N1–In1–O2 127.0(8).

ε-caprolactone (CL) using a 200 : 1 monomer to catalyst ratio in dichloromethane (DCM) at room temperature (Table 1). All complexes are highly active for the ROP of L-LA achieving 89–98% conversion within 3–5 min giving polylactide (PLA) with a narrow dispersity (*Đ* = 1.06–1.09) in entries 1–3. The molecular weights are generally larger than the expected molecular weight. The differences between theoretical and experimental molecular weights could be a result of a relatively slow initiation rate of the sterically hindered *tert*-butoxide initiator compared to the propagation rate leading to the polymerization of fewer chains than theoretical predictions as observed in many reports.[37,43]

Complex **2a** showed the slowest activity in the catalyst series for the ROP of L-LA (entry 1). On the other hand, complexes **2b** and **2c** were significantly faster taking only 3 min to achieve 96 and 98% conversion, respectively (entries 2 and 3). Notably, **2c** shows much higher activity (TOF = 3920 h^{-1}) than several other In alkoxide catalysts reported for ROP of lactide, such as in (salfen)In(O*t*Bu) and phosphasalen indium complexes (ave. TOF of 21–160 h^{-1}, see Fig. 1).[37,43] The geometry of **2b** and **2c** may enhance its efficiency compared to **2a**, as it is presumed to allow better access to the transition state during the ROP process.[57] Moreover, an excess of benzyl alcohol (5 equiv.) can be added to the ROP of L-LA using complex **2c**. The polymerization still proceeded very quickly finishing over 80% conversion in 3 min giving PLA with a narrow dispersity of 1.05 (entry 4). The molecular weight decreased in accordance with the added alcohol as the chain transfer agent. Complex **2c** remained active at a higher L-LA : **2c** ratio of 500 : 1, achieving 98% conversion in 10 min (entry 5) giving PLA with an M_n of 55.6 kDa (*Đ* = 1.03). At a higher monomer ratio, the molecular weight tends to match better with the expected molecular weight, as a longer polymerization time is given for the initiation step to proceed. To demonstrate the living nature of this catalyst, a sequential addition of L-LA was performed. Starting from the polymerization of 100 equiv. of L-LA by **2c** for 3 min (99% conversion at this point), the polymerization was stirred for an additional 15 min, followed by the addition of 50 equiv. of L-LA for 7 min (99% conversion). The molecular weight increased from 13.0 kDa to 22.6 kDa with narrow dispersity after the second portion of L-LA was added (Fig. S50). The ROP of GA was also carried out using **2c** (entry 6). After 5 min, full conversion of GA was observed with the precipitation of polyglycolide. The molecular weight and dispersity of polyglycolide (PGA) could not be determined due to the insolubility of polyglycolide in organic solvents. Complex **2c** was also highly active for the ROP of CL using a CL : **2c** ratio of 200 : 1 at room temperature giving 86% conversion in 15 min (entry 7).

Ring-opening polymerization of *rac*-lactide

Complexes **2a–2c**, featuring different diamine backbones, were investigated for stereoselectivity in ROP of *rac*-LA at room temperature (Table 2, entries 1–3). The polymerizations were very fast giving 70–90% conversion of 200 equiv. of *rac*-LA in 5–8 min at room temperature, where complex **2c** was the fastest. The polymerization time was slightly longer compared to the ROP of L-LA since a lower concentration (0.500 M) was used. The resulting PLAs have a narrow dispersity (*Đ* = 1.05–1.08) and surprisingly are highly isotactic with P_m values

Table 1 Ring-opening polymerization (ROP) of cyclic esters[a]

Entry	Monomer	Catalyst	Time (min)	Conv.[e] (%)	TOF[f] (h^{-1})	$M_{n,\,th}$[g] (kDa)	$M_{n,\,GPC}$[h] (kDa)	*Đ*[h]
1	L-LA	**2a**	5	89	2145	25.6	54.6	1.06
2	L-LA	**2b**	3	96	3840	27.8	44.5	1.06
3	L-LA	**2c**	3	98	3920	28.4	44.2	1.09
4[b]	L-LA	**2c**	3	83	3320	3.97	1.9	1.05
5[c]	L-LA	**2c**	10	98	2940	70.6	55.6	1.03
6[d]	GA	**2c**	5	>99	2410	—	—	—
7	CL	**2c**	15	86	688	19.7	37.9	1.34

[a] Reaction conditions: [M] : [In] = 200 : 1, $[M]_0$ = 1.00 M, DCM, RT. [b] Add 5 equiv. of benzyl alcohol. [c] [M] : [In] = 500 : 1, $[M]_0$ = 1.00 M, DCM, RT. [d] $[M]_0$ = 0.250 M, DCM, RT. [e] Conversion determined by ^{1}H NMR of a crude polymer sample. [f] TOF = (number of moles of LA consumed per mole of catalyst)/time (h). [g] $M_{n,th} = [M]_0/[In]_0 \times$ conversion $\times M_{monomer} + M_{initiator}$. [h] Determined by GPC analysis using a refractive index (RI) detector and polystyrene as a standard in THF with a correction factor of 0.58 for L-LA and 0.56 for ε-CL.

Table 2 Ring-opening polymerization (ROP) of *rac*-lactide[a]

Entry	Cat.	Time (min)	Conv.[c] (%)	$M_{n,th}$[d] (kDa)	$M_{n,GPC}$[e] (kDa)	$Đ$[e]	P_m[f]
1	**2a**	8	90	26.1	33.1	1.08	0.64
2	**2b**	5	70	20.3	30.5	1.05	0.66
3	**2c**	5	85	24.6	40.8	1.08	0.75
4[b]	**2c**	6 h	84	12.2	41.1	1.05	0.85

[a] Reaction conditions: [M] : [In] = 200 : 1, $[M]_0$ = 0.500 M, DCM, RT. [b] [M] : [In] = 100 : 1, $[M]_0$ = 0.100 M, DCM, −30 °C. [c] Conversion determined by ^{1}H NMR analysis of the crude polymer sample. [d] $M_{n,th}$ = $[M]_0/[In]_0$ × conversion × $M_{monomer}$ + $M_{Ot\text{-}Bu}$. [e] Determined by GPC analysis using a refractive index (RI) detector and polystyrene as a standard in THF with a correction factor of 0.58. [f] Determined by integration of PLA methine tetrads in the ^{1}H NMR spectrum using values predicted by Bernoulli statistics.

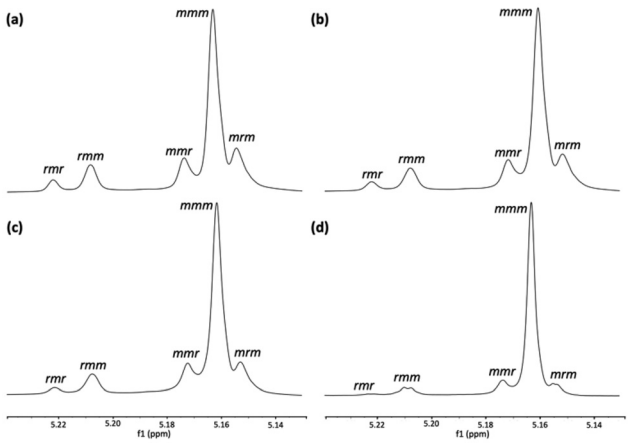

Fig. 5 A series of homonuclear ^{1}H-decoupled NMR (600 Hz, $CDCl_3$, 30 °C) in the methine region of poly(*rac*-LA) catalyzed by (a) **2a**, (b) **2b**, (c) **2c** at room temperature, and (d) **2c** at −30 °C.

ranging from 0.64 to 0.75 as analyzed by homonuclear decoupled ^{1}H NMR spectroscopy and Bernoulli statistics.[58] This is rather surprising since complexes **2a** and **2b** are achiral but still give highly isotactic PLA with similar P_m values of 0.64 and 0.66, respectively (Fig. 5a and b). On the other hand, chiral complex **2c** is the most isoselective giving PLA with a P_m value of 0.75 (Fig. 5c). Compared with other indium catalysts (Fig. 1),[35,37,40,43,44] complexes **2a** and **2b** produced moderate isotacticity. Previously reported indium catalysts exhibited P_m values ranging from 0.37 to 0.92. Ferrocenylsalen (salfen)In (O*t*Bu) (**A**) showed no tacticity control, forming atactic PLA with P_m = 0.52,[37] whereas polymers catalyzed by indium salan (**B**) were slightly heterotactic enriched P_r = 0.60–0.63.[40] Complex **2c** outperformed other indium catalysts including ferrocenylsalen and salan complexes in terms of activity and isoselectivity. However, the isoselectivity of complex **2c** remains lower than that of phosphasalen-related frameworks reported by Williams (P_m = 0.92)[3] and slightly lower than chiral salen complexes reported by Mehrkhodavandi (P_m = 0.77).[44] In general, there are 2 mechanisms for stereoselectivity: (i) enantiomorphic site control (ESC), in which chiral catalysts selectively react with one lactide enantiomer and (ii) chain-end control (CEC), in which achiral catalysts induce stereocontrol through interactions with the terminal group of the growing polymer chains.[59] An example of the latter was reported by Nomura and coworkers where achiral Al-salen catalysts showed high isoselectivity by chain end-control mechanisms.[60] Since complexes **2a** and **2b** are achiral, their stereoselectivity may likely proceed *via* the chain-end control mechanism. When the polymerization of *rac*-LA was catalyzed by chiral complex **2c** at −30 °C (Table 3, entry 4), the polymerization finished in 6 h giving highly isotactic PLA with an increased P_m value of 0.85 (Fig. 5d). At such high isoselectivity, the analysis of *rmr*, *rmm*, *mmr*, and *mrm* tetrads in this polymer could give some information about the origin of the stereoselectivity in this catalyst. If the stereoerrors occurred from misinsertion of enantiomers to the chiral catalyst (enantiomorphic site control), the integration ratio of *rmr* : *rmm* : *mmr* : *mrm* is 1 : 1 : 1 : 2. On the other hand, if the stereoerrors occurred within the chain-end control, the integration ratio of *rmr* : *rmm* : *mmr* : *mrm* would be 0 : 1 : 1 : 1.[61] From the homonuclear decoupled ^{1}H NMR spectrum of PLA in Table 2 entry 4, the integration ratio of *rmm*, *mmr*, and *mrm* tetrads is nearly 1 : 1 : 1 while that of the *rmr* tetrad is negligible (Fig. 5d and S10). This observation is consistent with the chain-end control being the major source of stereoselectivity. This result is also in line with the observed isoselectivity by achiral complexes **2a** and **2b** where the chain-end control is likely operative. The analysis of the polymer end-group using a low [*rac*-LA] : [**2c**] ratio of 10 : 1 by MALDI-TOF mass spectrometry revealed the mass series of 1 + $(144)_n$ + 73 + 23 assignable to H[*rac*-LA]$_n$O^{t}Bu + Na^+ confirming that the polymerization was initiated by a *tert*-butoxide with minimal transesterifications (Fig. S18).

Kinetic studies

Catalyst **2c** being the most isoselective was further investigated for kinetic studies for L-LA, D-LA, *rac*-LA, and CL. The rates of polymerization for each monomer can be compared using the rate coefficients (k_{obs}). All polymerizations were carried out in triplicate using [monomer] : [**2c**] = 200 : 1 with an initial monomer concentration of 0.500 M in DCM at room temperature. Conversion was determined using NMR spectroscopy by taking aliquots at different time intervals (Fig. S19). A plot of $\ln([M]_0/[M]_t)$ of all monomers showed a linear fit with the reaction time consistent with a pseudo first-order reaction with respect to monomer concentration (Fig. 6). k_{obs}'s are in the order *rac*-LA (0.404 min^{-1}) ≈ D-LA (0.403 min^{-1}) > L-LA (0.214 min^{-1}) ≫ ε-CL (0.057 min^{-1}). The difference in the polymerization rates of D-LA and L-LA may be caused by the enantioselectivity toward D-LA from the ligand chirality of **2c**. Moreover, the higher polymerization rate of D-LA over L-LA ($k_{D\text{-}LA}/k_{L\text{-}LA}$ = 1.9) indicated that the enchainment of D-LA in the ROP of *rac*-LA is preferred.[62] This result deviates from our predictions. Since the diamine backbone of the catalyst is also chiral, the stereoselectivity may also be further influenced by

Table 3 Copolymerization of cyclic esters using complex **2c**

	Monomer													
Entry	A	B	Time (min)	A conv.[c] (%)	B conv.[c] (%)	A : B ratio[d]	L_A[e]	L_B[e]	r_A[f]	r_B[f]	$M_{n,th}$[g] (kDa)	$M_{n,GPC}$[h] (kDa)	$Đ$[h]	T_g[i] (°C)	T_m[i] (°C)
1[a]	L-LA	GA	5	82	>99	73 : 27	15.8	7.9	3.7	27.6	23.6	81.2	1.38	47	n/a
2[a]	D-LA	GA	5	95	>99	78 : 22	17.9	6.7	4.2	22.8	26.6	74.4	1.68	48	149
3[b]	L-LA	CL	1 d	>99	61	65 : 35	3.4	1.8	2.4	0.8	21.4	42.5	1.68	6	126
4[b]	D-LA	CL	1 d	>99	79	56 : 44	2.5	1.7	1.5	0.7	23.5	54.0	1.76	−4	n/a

[a] Reaction conditions: [LA] : [GA] : [**2c**] = 160 : 40 : 1, $[LA]_0$ = 0.5 M, DCM, RT. [b] Reaction conditions: [LA] : [CL] : [**2c**] = 100 : 100 : 1, $[LA]_0$ = 0.5 M, DCM, RT. [c] Conversion determined by ^{1}H NMR analysis of the crude polymer sample. [d] Incorporation ratio of A : B in the purified copolymer determined by ^{1}H NMR spectroscopy. [e] L_A: the average length of the carbonyl region of monomer A; L_B: the average length of the carbonyl region of monomer B, determined by the ^{13}C NMR spectrum of the purified polymer sample; see more details in the SI. [f] r_A: the reactivity ratio of monomer A; r_B: the reactivity ratio of monomer B; see more details in the SI. [g] $M_{n,th}$ = $[M]_0/[In]_0$ × conversion × $M_{monomer}$ + $M_{Oi\text{-}Bu}$. [h] Determined by GPC analysis using a refractive index (RI) detector and polystyrene as a standard in THF. [i] T_g and T_m were determined by DSC analysis at a heating rate of 10 °C min^{-1}.

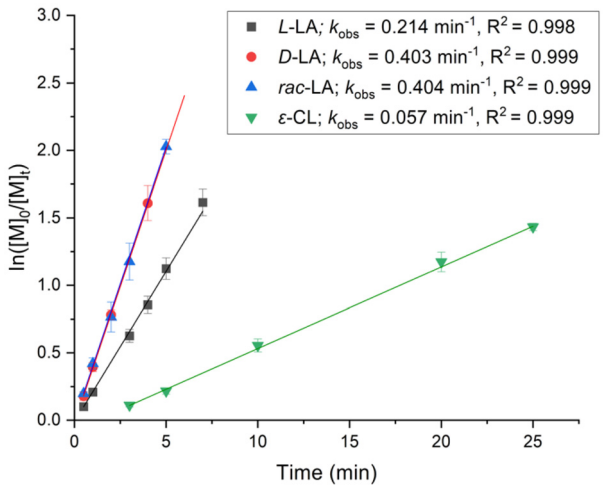

Fig. 6 Plot of ln([M]$_0$/[M]$_t$) *vs.* reaction time. Conditions: [M] : [**2c**] = 200 : 1 and $[M]_0$ = 0.500 M in DCM, RT at different times.

the ESC mechanism to some extent. It is possible that both ESC and CEC mechanisms may play a role in giving a more complex polymerization rate toward *rac*-, L- and D-LA. There have been several reports of the mixture of ESC and CEC mechanisms both in operation within the same catalyst system.[25,62,63]

Copolymerization of cyclic esters

Complex **2c** was further investigated for the solution copolymerization of cyclic esters. Typically, the ROP of GA is performed in bulk polymerization (150–230 °C)[5,6] or in a fluorinated solvent such as hexafluoroisopropanol[64] due to the poor solubility of PGA in common organic solvents. Copolymerization of LA and GA in DCM was challenging due to the insolubility of polyglycolide at the initial stage of the polymerization causing immediate polymer precipitation. After several attempts, we found that the maximum mole ratio of GA in the copolymerization with LA was 20% to still keep the copolymer in solution (see Table S1). Therefore, the copolymerizations of GA with L-LA and D-LA using an [LA] : [GA] : [**2c**] ratio of 160 : 40 : 1 were carried out in DCM at RT (Table 3, entries 1–2). For both L-LA and D-LA, the copolymerization proceeded efficiently within 5 min. GA was consumed more rapidly giving >99% conversion while some LA remained. At the same polymerization time, the conversion of D-LA (95%) was higher than that of L-LA (82%). This result is in line with the faster kinetic result for D-LA compared to L-LA. A similar trend was observed for the copolymerization of LA with CL, carried out for one day using a [LA] : [CL] : [**2c**] mole ratio of 100 : 100 : 1 (Table 3, entries 3 and 4). Lactide was completely consumed while some CL remained. The difference in polymerization rates between homo- and copolymerizations was observed earlier and can be attributed to the stable five-membered ring between the metal and the closest ester group after LA was inserted.[65,66] This chelation slows down the ROP when the next monomer is CL. DOSY NMR of the copolymers (both LA/GA and LA/CL) gave a single diffusion coefficient confirming the copolymer nature of LA/GA and LA/CL (Fig. S23, S27, S31, and S35). The structural sequence of all copolymers was analyzed by ^{1}H and ^{13}C NMR spectroscopy (Fig. S20–S35).[6,51–53] Carbonyl signals of each monomer sequence were assigned, and the average block lengths of lactyl (L_{LA}), glycolyl (L_{GA}), and caproyl (L_{CL}) units were calculated. From these data, the monomer reactivity ratios were determined. When the reactivity ratios of both monomers A (r_A) and B (r_B) are greater than 1, block copolymers are formed. In contrast, when $r_A > 1$ and $r_B < 1$ ($r_A > 1 > r_B$), the formation of gradient copolymers is favorable.[67,68] The copolymerization of LA and GA yielded r_{LA} of 3.7–4.2 and r_{GA} of 22.8–27.6, consistent with block copolymer formation. On the other hand, the copolymerization of LA and CL produced r_{LA} of 1.5–2.4 and r_{CL} of 0.7–0.8, indicative of a gradient copolymer. The actual incorporation ratios of A : B monomers in all purified copolymers agree well with the conversion of each monomer (entries 1–4). The thermal properties of the copolymers were measured by DSC. The glass transition temperatures (T_g) of the LA/GA block copolymer in entries 1 and 2 are 47 °C and 48 °C, respectively, within the range of T_g for isotactic PLA (45–65 °C).[69,70] A single T_g for the LA/CL copolymer was also found at 6 and −4 °C for entries 3 and 4, respectively. This single T_g of the LA/CL copolymer is intermediate between that of PCL[7] (T_g −65 to −60 °C) and of PLA[69,70] (T_g 45–65 °C) in agreement with the gradient copolymer.

Conclusions

A series of indium *tert*-butoxide complexes supported by constrained inden ligands **2a–2c** were successfully synthesized and characterized. All complexes were demonstrated as efficient catalysts for the ROP of cyclic esters giving high molecular weight polymers with narrow dispersity. Complex **2c** containing a (±)-*trans*-cyclohexyl backbone was highly active in the ROP of lactide, finishing conversion of 200 equiv. of lactide in 3 min. All complexes were investigated for isoselectivity in the ROP of *rac*-LA giving stereoblock isotactic-enriched PLA with P_m values up to 0.75 at room temperature and 0.85 at −30 °C. Chain-end control was proposed to be responsible for the isoselectivity of the catalysts. Copolymerization of LA with GA gave block copolymers while the copolymerization of LA with CL gave gradient copolymers. This work highlights the potential of modifiable ligands containing a constrained five-membered ring at the imine position to enhance both the polymerization rate and stereoselectivity in the ROP of cyclic esters.

Author contributions

K. Phomphrai: conceptualization, supervision, and writing – review & editing. P. Chumsaeng: single crystal X-ray analysis and refinement of the structures. T. Piyawongsiri: investigation, methodology, and writing – original draft. All authors have given approval to the final version of the manuscript.

Conflicts of interest

There are no conflicts to declare.

Data availability

The data supporting this article have been included as part of the supplementary information (SI). Supplementary information is available. See DOI: https://doi.org/10.1039/d5dt02356d.

CCDC 2489168–2489170 contain the supplementary crystallographic data for this paper.[71a–c]

Acknowledgements

Financial support from the Vidyasirimedhi Institute of Science and Technology (M22KHP-VIS010) and the National Research Council of Thailand (NRCT) (No. N42 A650196) is gratefully acknowledged. The authors also acknowledge financial support from the Thailand Science Research and Innovation (FRB680014/0457) and the Program Management Unit for Human Resources & Institutional Development, Research and Innovation (Grant Number: B41G680026, Global League). Support for scientific instruments from the Frontier Research Center, VISTEC, is gratefully acknowledged.

References

1 P. Rychter, M. Kawalec, M. Sobota, P. Kurcok and M. Kowalczuk, *Biomacromolecules*, 2010, **11**, 839–847.
2 B. R. E. Drumright, P. R. Gruber and D. E. Henton, *Adv. Mater.*, 2000, **12**, 1841–1846.
3 A. P. Gupta and V. Kumar, *Eur. Polym. J.*, 2007, **43**, 4053–4074.
4 Y. Zhu, C. Romain and C. K. Williams, *Nature*, 2016, **540**, 354–362.
5 O. Dechy-Cabaret, B. Martin-Vaca and D. Bourissou, *Chem. Rev.*, 2004, **104**, 6147–6176.
6 P. K. Samantaray, A. Little, D. M. Haddleton, T. McNally, B. Tan, Z. Sun, W. Huang, Y. Ji and C. Wan, *Green Chem.*, 2020, **22**, 4055–4081.
7 M. Labet and W. Thielemans, *Chem. Soc. Rev.*, 2009, **38**, 3484–3504.
8 H. R. Kricheldorf, M. Berl and N. Scharnagl, *Macromolecules*, 1988, **21**, 286–293.
9 R. Auras, B. Harte and S. Selke, *Macromol. Biosci.*, 2004, **4**, 835–864.
10 M. Rabnawaz, I. Wyman, R. Auras and S. Cheng, *Green Chem.*, 2017, **19**, 4737–4753.
11 E. Castro-Aguirre, F. Iñiguez-Franco, H. Samsudin, X. Fang and R. Auras, *Adv. Drug Delivery Rev.*, 2016, **107**, 333–366.
12 S. Bujok, J. Peter, M. Halecký, P. Ecorchard, A. Machálková, G. Santos Medeiros, J. Hodan, E. Pavlova and H. Beneš, *Polym. Degrad. Stab.*, 2021, **190**, 109625.
13 B. D. Ulery, L. S. Nair and C. T. Laurencin, *J. Polym. Sci., Part B: Polym. Phys.*, 2011, **49**, 832–864.
14 N. Mhlanga, S. Sinha Ray, Y. Lemmer and J. Wesley-Smith, *ACS Appl. Mater. Interfaces*, 2015, **7**, 22692–22701.
15 D. J. A. Cameron and M. P. Shaver, *Chem. Soc. Rev.*, 2011, **40**, 1761–1776.
16 D. K. Gilding and A. M. Reed, *Polymers*, 1979, **20**, 1459–1464.
17 A.-C. Albertsson and I. K. Varma, *Biomacromolecules*, 2003, **4**, 1466–1486.
18 K. Budak, O. Sogut and U. A. Sezer, *J. Polym. Res.*, 2020, **27**, 208.
19 C. Jian, J. Zhang, Z. Dai, Y. Gao, N. Tang and J. Wu, *Eur. J. Inorg. Chem.*, 2013, **2013**, 3533–3541.
20 J. Hu, C. Kan, H. Wang and H. Ma, *Macromolecules*, 2018, **51**, 5304–5312.
21 M.-L. Shueh, Y.-S. Wang, B.-H. Huang, C.-Y. Kuo and C.-C. Lin, *Macromolecules*, 2004, **37**, 5155–5162.
22 S. Abbina and G. Du, *ACS Macro Lett.*, 2014, **3**, 689–692.
23 D. E. Stasiw, A. M. Luke, T. Rosen, A. B. League, M. Mandal, B. D. Neisen, C. J. Cramer, M. Kol and W. B. Tolman, *Inorg. Chem.*, 2017, **56**, 14366–14372.
24 N. Nomura, R. Ishii, Y. Yamamoto and T. Kondo, *Chem. – Eur. J.*, 2007, **13**, 4433–4451.
25 A. Pilone, K. Press, I. Goldberg, M. Kol, M. Mazzeo and M. Lamberti, *J. Am. Chem. Soc.*, 2014, **136**, 2940–2943.

26 P. Chumsaeng, S. Haesuwannakij, A. Virachotikul and K. Phomphrai, *J. Polym. Sci., Part A:Polym. Chem.*, 2019, **57**, 1635–1644.
27 C.-M. Dong, K.-Y. Qiu, Z.-W. Gu and X.-D. Feng, *Macromolecules*, 2001, **34**, 4691–4696.
28 C. W. Vos, J. Beament and C. M. Kozak, *Polym. Chem.*, 2023, **14**, 5083–5093.
29 B. J. O'Keefe, M. A. Hillmyer and W. B. Tolman, *J. Chem. Soc., Dalton Trans.*, 2001, 2215–2224.
30 J. Wu, T.-L. Yu, C.-T. Chen and C.-C. Lin, *Coord. Chem. Rev.*, 2006, **250**, 602–626.
31 J. Gao, D. Zhu, W. Zhang, G. A. Solan, Y. Ma and W.-H. Sun, *Inorg. Chem. Front.*, 2019, **6**, 2619–2652.
32 D. Xu, Y. Xu, H. Wang and X. Qiu, *Chem. Commun.*, 2022, **58**, 3007–3010.
33 B. Pan, G. Yuan, X. Zhao, N. Han, Y. Huang, K. Feng, C. Cheng, J. Zhong, L. Zhang, Y. Wang and Y. Li, *Small Sci.*, 2021, **1**, 2100029.
34 N. Maudoux, T. Roisnel, V. Dorcet, J. F. Carpentier and Y. Sarazin, *Chem. – Eur. J.*, 2014, **20**, 6131–6147.
35 D. Myers, A. J. P. White, C. M. Forsyth, M. Bown and C. K. Williams, *Angew. Chem., Int. Ed.*, 2017, **56**, 5277–5282.
36 A. Thevenon, A. Cyriac, D. Myers, A. J. P. White, C. B. Durr and C. K. Williams, *J. Am. Chem. Soc.*, 2018, **140**, 6893–6903.
37 S. M. Quan and P. L. Diaconescu, *Chem. Commun.*, 2015, **51**, 9643–9646.
38 K. Hosseini, C. Goonesinghe, H. Roshandel, J. Chang, K. Nyamayaro, H.-J. Jung, P. L. Diaconescu and P. Mehrkhodavandi, *ACS Catal.*, 2023, **13**, 13195–13204.
39 M. Martínez de Sarasa Buchaca, F. de la Cruz-Martínez, L. F. Sánchez-Barba, J. Tejeda, A. M. Rodríguez, J. A. Castro-Osma and A. Lara-Sánchez, *Dalton Trans.*, 2023, **52**, 3482–3492.
40 J. Bruckmoser, D. Henschel, S. Vagin and B. Rieger, *Catal. Sci. Technol.*, 2022, **12**, 3295–3302.
41 A. Pietrangelo, M. A. Hillmyer and W. B. Tolman, *Chem. Commun.*, 2009, 2736–2737.
42 A. Pietrangelo, S. C. Knight, A. K. Gupta, L. J. Yao, M. A. Hillmyer and W. B. Tolman, *J. Am. Chem. Soc.*, 2010, **132**, 11649–11657.
43 N. Yuntawattana, T. M. McGuire, C. B. Durr, A. Buchard and C. K. Williams, *Catal. Sci. Technol.*, 2020, **10**, 7226–7239.
44 D. C. Aluthge, J. M. Ahn and P. Mehrkhodavandi, *Chem. Sci.*, 2015, **6**, 5284–5292.
45 T. Piyawongsiri, N. Laiwattanapaisarn, A. Virachotikul, P. Chumsaeng and K. Phomphrai, *ChemPlusChem*, 2023, **88**, e202300559.
46 J. Kiriratnikom, N. Laiwattanapaisarn, K. Vongnam, N. Thavornsin, P. Sae-Ung, S. Kaeothip, A. Euapermkiati, S. Namuangruk and K. Phomphrai, *Inorg. Chem.*, 2021, **60**, 6147–6151.
47 N. Laiwattanapaisarn, A. Virachotikul and K. Phomphrai, *Dalton Trans.*, 2021, **50**, 11039–11048.
48 N. Laiwattanapaisarn, A. Virachotikul, P. Chumsaeng, T. Jaenjai and K. Phomphrai, *Inorg. Chem.*, 2022, **61**, 20616–20628.
49 G. M. Sheldrick, *Acta Crystallogr., Sect. C: Struct. Chem.*, 2015, **71**, 3–8.
50 O. V. Dolomanov, L. J. Bourhis, R. J. Gildea, J. A. K. Howard and H. Puschmann, *J. Appl. Crystallogr.*, 2009, **42**, 339–341.
51 D. A. Atwood and M. J. Harvey, *Chem. Rev.*, 2001, **101**, 37–52.
52 D. C. Aluthge, B. O. Patrick and P. Mehrkhodavandi, *Chem. Commun.*, 2013, **49**, 4295–4297.
53 A. W. Addison, T. N. Rao, J. Reedijk, J. van Rijn and G. C. Verschoor, *Dalton Trans.*, 1984, 1349–1356.
54 K.-Y. Chen, Y.-S. Wen, T.-C. Fang, Y.-J. Chang and M.-J. Chang, *Acta Crystallogr., Sect. E:Struct. Rep. Online*, 2011, **67**, 927.
55 K. Kitamura, Y. Ando, T. Matsumoto and K. Suzuki, *Angew. Chem., Int. Ed.*, 2014, **53**, 1258–1261.
56 T. A. Olszak, A. Stepien, E. Wajsman and M. J. Grabowski, *Acta Crystallogr., Sect. B*, 1980, **36**, 2850–2851.
57 P. Hormnirun, E. L. Marshall, V. C. Gibson, R. I. Pugh and A. J. P. White, *Proc. Natl. Acad. Sci. U. S. A.*, 2006, **103**, 15343–15348.
58 B. M. Chamberlain, M. Cheng, D. R. Moore, T. M. Ovitt, E. B. Lobkovsky and G. W. Coates, *J. Am. Chem. Soc.*, 2001, **123**, 3229–3238.
59 M. J. Stanford and A. P. Dove, *Chem. Soc. Rev.*, 2010, **39**, 486–494.
60 N. Nomura, R. Ishii, M. Akakura and K. Aoi, *J. Am. Chem. Soc.*, 2002, **124**, 5938–5939.
61 T. M. Ovitt and G. W. Coates, *J. Polym. Sci., Part A:Polym. Chem.*, 2000, **38**, 4686–4692.
62 H. Wang and H. Ma, *Chem. Commun.*, 2013, **49**, 8686–8688.
63 M. H. Chisholm, N. J. Patmore and Z. Zhou, *Chem. Commun.*, 2005, 127–129.
64 P. Zhang, V. Ladelta and N. Hadjichristidis, *J. Am. Chem. Soc.*, 2023, **145**, 14756–14765.
65 M. Keram and H. Ma, *Appl. Organomet. Chem.*, 2017, **31**, e3893.
66 S. Ghosh, E. Glöckler, C. Wölper, A. Tjaberings, A. H. Gröschel and S. Schulz, *Dalton Trans.*, 2020, **49**, 13475–13486.
67 P. Vanhoorne, P. Dubois, R. Jerome and P. Teyssie, *Macromolecules*, 1992, **25**, 37–44.
68 B. S. Beckingham, G. E. Sanoja and N. A. Lynd, *Macromolecules*, 2015, **48**, 6922–6930.
69 A. Z. Naser, I. Deiab and B. M. Darras, *RSC Adv.*, 2021, **11**, 17151–17196.
70 D. Garlotta, *J. Polym. Environ.*, 2001, **9**, 63–84.
71 (*a*) CCDC 2489168: Experimental Crystal Structure Determination, 2025, DOI: 10.5517/ccdc.csd.cc2pk5r6; (*b*) CCDC 2489169: Experimental Crystal Structure Determination, 2025, DOI: 10.5517/ccdc.csd.cc2pk5s7; (*c*) CCDC 2489170: Experimental Crystal Structure Determination, 2025, DOI: 10.5517/ccdc.csd.cc2pk5t8.